IN SITU CHEMICAL MODIFICATION OF C-S-H INDUCED BY CO_2 LASER IRRADIATION

Sagrario Martínez-Ramírez[a,1]; Luis Diaz[a]; Moisés Martín-Garrido[a]; Lucia Fernández-Carrasco[b] and David Torrens[b]

[a]Instituto de Estructura de la Materia, (IEM-CSIC)

Sagrario Martínez-Ramírez ORCID: 0000-0002-6322-535X

C/Serrano 121, 28006 Madrid. Spain

[b]Escuela Técnica Superior de Ingenieros de Caminos, Canales y Puertos de Barcelona Universitat Politècnica de Catalunya

Lucia Fernández Carrasoc ORCID: 0000-0002-2379-3782

107 Calle Jordi Girona, 1-3. 08034 Barcelona

ABSTRACT

Fire-induced compositional changes lead to strength loss and even failure in cement and concrete. Calcium silicate hydrate (C-S-H) gel, the main product of cement hydration, dehydrates at 25 °C to 200 °C, while temperatures of 850 °C to 900 °C alter its structure. A Raman spectroscopic study of the amorphous and crystalline phases forming after CO_2 laser radiation of cement mortar showed that C-S-H dehydration yielded tricalcium silicate at higher, and dicalcium silicate at lower, temperatures. Post-radiation variations were identified in the position of the band generated by Si-O bond stretching vibrations.

Keywords: Microstructure; calcium silicate hydrate; spectroscopy; degradation; Ca_2SiO_4*;* Ca_2SiO_5*.*

[1] Corresponding author: Sagrario Martínez-Ramírez, Instituto de Estructura de la Materia, C/Serrano 121, 28006 Madrid (Spain). Tfno: +34 915616800; Fax: +34 915645557. sagrario.martinez@csic.es

INTRODUCTION

Concrete is a fairly non-combustible, fire-safe material that resists high temperatures well. Fire nonetheless poses a severe risk to concrete buildings and structures, inducing structural weakening [1] as well as physical changes such as spalling and colour loss [2] attributable to chemical processes governed by material composition and the temperatures reached [3].

Concrete strength declines with rising temperatures. At 100 ° to 200 °C the vapour pressure ensuing from free water evaporation prompts spalling, whereas at 300 °C non-evaporative water loss reduces strength by 15 % to 40 % [1,4,5]. Decay is most intense at 600 °C or over, when concrete compressive strength drops to 7 % to 25 % of the initial value.

The effect of heat on the composition of the primary binder in concrete, cement, is likewise temperature-dependent [6]: calcium silicate hydrate (C-S-H) dehydrates at 80 °C to 100 °C; calcium sulfoaluminate hydrate (ettringite) decomposes at 60 °C to 80 °C; calcium hydroxide dehydrates at around 400 °C; and calcium carbonate decomposes at 600 °C to 900 °C. Incipient melting is observed at 1100 °C. The change in free water from liquid to gas at that temperature varies the rate of heat transmission from the concrete surface to its interior.

C-S-H gel, the majority chemical compound in hydrated cement, precipitates as a disorderly, metastable, amorphous structure similar to tobermorite ($Ca_5Si_6O_{16}(OH)$. When heated, tobermorite converts into stable, highly crystalline phases. According to Shaw et al. [6], at 840 °C to 855 °C it dehydrates and restructures into wollastonite ($CaSiO_3$). In a recent study, Tajuelo-Rodríguez et al. [7] determined that the temperature at which C-S-H converts into β-wollastonite rises with the Ca/Si ratio in the gel.

Since the physics of the heat generated by photo-physical reactions is similar to the physics of fire, laser radiation has been used to study the effect of fire on building

materials [8, 9]. In a prior study by the authors [10], portlandite and a vitreous material were observed to form in a continuous wave CO_2 laser- (CW CO_2 laser) irradiated lime pozzolan mortar containing calcium carbonate as the main binder and a small fraction of calcium silicate. In belite cement synthesis, with high dicalcium silicate, hydrothermal procedures are applied to form hydrated phases which are subsequently calcined to extract dicalcium silicate [11]. In other words, heat is applied to hydrated phases to synthesise anhydrous calcium silicates with the same Ca/Si ratio.

Raman spectroscopy, used to analyse short-range order and local bonding in materials, is also very useful for characterising materials containing both amorphous and crystalline phases, such as cement, mortar and concrete [12-15]. Moreover, the technique requires no sample preparation and only a few milligrams of the substance to be analysed. The main drawback to Raman spectroscopy is the background noise generated by fluorescence attributable to impurities and rough surface-induced elastic scattering, which overlaps with the Raman peaks associated with cement compounds. Such fluorescence, which Newman et al. [16] suggested may be associated in portland cement with silicate phase polymerisation, can be minimised with low excitation frequency micro-Raman [10].

This study explored the chemistry of calcium silicate hydrate conversion to di- and tricalcium silicate to determine whether these or other calcium silicates formed when cement samples were exposed to high temperatures. High temperatures were simulated in the samples by irradiating cement mortar with a CO_2 laser [17]. Micro-Raman spectroscopy was used to monitor the amorphous and crystalline phases present in the samples analysed.

EXPERIMENTAL

Materials

Type I cement and silica (SiO_2) aggregate were used to prepare the mortar specimens. X-ray fluorescence showed the main cement constituents to be SiO_2 (18.50 %), CaO

(57.75 %), Al_2O_3 (4.55 %), Fe_2O_3 (3.50 %) and SO_3 (7.69 %). Loss on ignition at 1000 °C was 3.5 %. The SiO_2 content in the siliceous sand was 98.92 %. The X-ray diffraction (XRD) patterns for the initial cement showed that the typical majority constituents, calcium silicate compounds tricalcium silicate (C_3S)[2] and dicalcium silicate (C_2S) were found together with smaller amounts of calcium aluminate, C_3A, C_4AF, gypsum and anhydrite. Quartz was used as aggregate.

The raw materials were blended at a cement/aggregate ratio of 1/3 and mixed with water at a water/cement ratio of 0.25 to prepare 1x1x6 cm mortar specimens that were cured for 50 d at 21 °C and 99 % relative humidity. After 50 days, the hydration reaction was stopped by the addition of acetone/ethanol. The diffractogram for the mortar (ground to a particle size of 45 μm) reproduced in Figure 1 showed portlandite and calcite to be the majority crystalline phases. An amorphous hump at 2θ=30°-40° was attributed to C-S-H formation. The intensity of the C_3S signals was lower than in the pattern for the dry materials as a result of hydration.

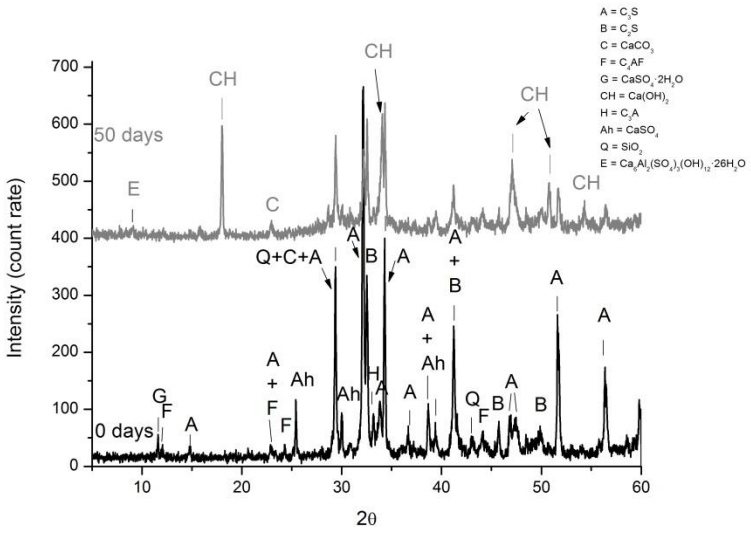

Fig. 1.- XRD patterns for anhydrous and 50 d hydrated cement

A = C_3S; B = C_2S; C =$CaCO_3$; F = C_4AF; G = $CaSO_4{\cdot}2H_2O$; CH = $Ca(OH)_2$; H = C_3A; Ah = $CaSO_4$; Q = SiO_2; E = $Ca_6Al_2(SO_4)_3(OH)_{12}{\cdot}26H_2O$

[2] Cement chemistry notation: C = CaO; S = SiO_2; H = H_2O; A = Al_2O_3; F = Fe_2O_3

CO_2 laser exposure

A CW CO_2 laser was used to irradiate the mortar to simulate fire effect. The irradiation was carried out with a CW (Firestar t80) CO_2 laser operating at a wavelength of 10.591 µm, 10P(20) CO_2 laser line as described elsewhere [10]. This laser has a maximum power output of 80 W, but in our experiments, laser output was kept at 14, 20, 30, 50, 70, 78 and 80 W as measured with a Synrad PW-250 power meter.

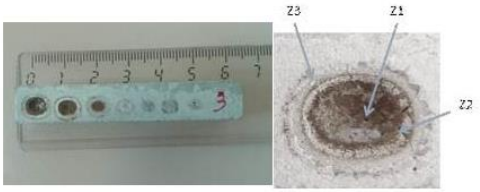

Figure 2.- Irradiated OPC mortar: a) laser power, from left to right, OPC-7 = 80 W; OPC-6 = 78 W; OPC-5 = 70 W; OPC-4 = 50 W; OPC-3 = 30 W; OPC-2 = 20 W; OPC-1 = 14 W; b) magnification of OPC-7 showing inner core (Z1); intermediate ring (Z2); and outer crown (Z3).

The unfocused laser beam was directed onto the surface of the sample by using gold coated mirrors. Irradiation time was 5 seconds. In this way, the energy delivered to the surface sample ranges between 70 and 2580 J. Irradiation of the mortar samples with the CW CO2 was made in air.

After melting under laser radiation, an indication that the temperature reached was higher than its 1450 °C melting point [17], the mortar surface cooled into an amorphous mass.

The general view of the samples after laser irradiation is depicted in Figure 2, whilst exposure time, output power and spot diameter are summarised in Table 1. Spot diameter was defined as the diameter of the vitreous (brown) area of the spot measured with a precision calliper. Spot size increased with laser power, peaking in sample OPC-7, irradiated at 80 W for 5 s. Spot borders were too indistinct in the samples irradiated at less than 30 W (see Figure 2) to determine the diameter.

Table 1. CO_2 laser exposure conditions and spot size

Sample	Exposure time (s)	Laser power (W)	Spot dia-meter (mm)
OPC-1	5	14	N.D.
OPC-2	5	20	N.D.
OPC-3	5	30	1.8
OPC-4	5	50	2.1
OPC-5	5	70	3.9
OPC-6	5	78	5.5
OPC-7	5	80	6.4

Micro-Raman spectroscopy

A confocal Raman microscope (Renishaw Invia 2000) equipped with a Leica microscope and an electrically refrigerated CCD camera was used to collect the Raman spectra. Laser excitation lines were provided by a diode laser (785 nm) and a Renishaw Nd;YAG laser (532 nm). The 5 mW laser beam was focused on different zones of the irradiated spots. The spectra were recorded using 50x objective lenses and an integration time of 10 s. WIRE for Windows and Galactic Industries GRAMS/32TM software were used for data acquisition and Origin 8.0 for analysis. Several zones were scanned in each spot, working from core to crown, with five scans recorded in each zone to enhance the signal-to-noise ratio. Daily calibration of the wavenumber axis was achieved by recording the Raman peak of silicon at 520 cm^{-1}. Spectra were normalized to the maximum intensity. Three spectra were analysed in z1 and z2.

X-Ray diffraction

X-ray diffraction (XRD) was conducted on a Bruker D8 Avance diffractometer fitted with a copper anode X-ray tube operating at 40 kV and 30 mA at diffraction angles ranging from 5° to 60° with a step speed of 0.038 s^{-1}.

RESULTS AND DISCUSSION

As high fluorescence hindered signal detection on the Raman spectra for the non-irradiated samples, they are not shown. Only one small band at 1085 cm^{-1} attributed to calcium carbonate was observed on the 532 nm laser spectrum and just one signal at 3616 cm^{-1} generated by portlandite on the 785 nm spectrum, whereas according to the XRD patterns the binder in the starting mortar contained C_3S, C_2S, C_4AF, C_3A, gypsum, anhydrite and calcite and the aggregate, quartz.

Three zones were distinguished in the spots generated: a central vitreous core (Z1), a thin brown ring around the core (Z2) and a wider outer crown (Z3). The differences in colour in the three zones were an indication that the peak temperature varied radially [18] (Figure 2).

The signals on the Raman spectrum for sample OPC-1, irradiated for 5 s at 14 W, varied depending on the zone (Figure 3). In Z1, where the laser impacted the surface, six bands were observed at 356 cm^{-1}, 453 cm^{-1}, 618 cm^{-1}, 980 cm^{-1}, 1004 cm^{-1} and 1070 cm^{-1}.

The band at 356 cm^{-1} was attributed to portlandite, a phase identified in previous studies on CO_2 laser-irradiated mortars and stones [8, 10]. The bands at 1004 cm^{-1} and 618 cm^{-1} were associated with gypsum ($CaSO_4 \cdot 2H_2O$), known to lose two water molecules at 220 °C, yielding thermodynamically metastable anhydrite III ($CaSO_4$). Insoluble anhydrite II forms at approximately 300 °C, with a very low rehydration rate depending on the peak temperature. Anhydrite I, a high temperature variety of anhydrite, is stable at >1180 °C [19], for at high temperatures and steep temperature ramping, a layer of oxides forming with $CaSO_4$ decomposition acts as a protective coating that detains the process [20]. Sanz [20] contended that anhydrite II can be hydrated with water vapour, whereas anhydrite I hydration calls for higher concentrations of water. The presence of gypsum in Z1 attested to the formation of anhydrite II and its hydration with water vapour.

As the majority compounds in the unexposed mortar were quartz and the calcium silicates C_3S and C_2S, the bands located at 453 cm^{-1}, 980 cm^{-1} and 1070 cm^{-1} may be thought to have been generated by a silicate. The main SiO_4 stretching bands lie at 800 cm^{-1} to 1200 cm^{-1}, depending on the position of the tetrahedron in the network. Isolated SiO_4 molecules generate signals at 800 cm^{-1} to 850 cm^{-1}, dimers at 950 cm^{-1}, silicate chains at 1050 cm^{-1} to 1100 cm^{-1}, silicate sheets at 1100 cm^{-1} and tectosilicates at 1150 cm^{-1} to 1250 cm^{-1}. The broad bands peaking at 980 cm^{-1} and 1070 cm^{-1} on the spectra for the exposed samples were respectively attributed to non-linked Si-O antisymmetric stretching and tetrahedral Si-O symmetrical stretching vibrations. The signal at 453 cm^{-1} was associated with non-crystalline SiO_2, which forms at temperatures of over 540 °C [22], and that can be assumed that it has been formed from the quartz may that have been melted (1710 °C).

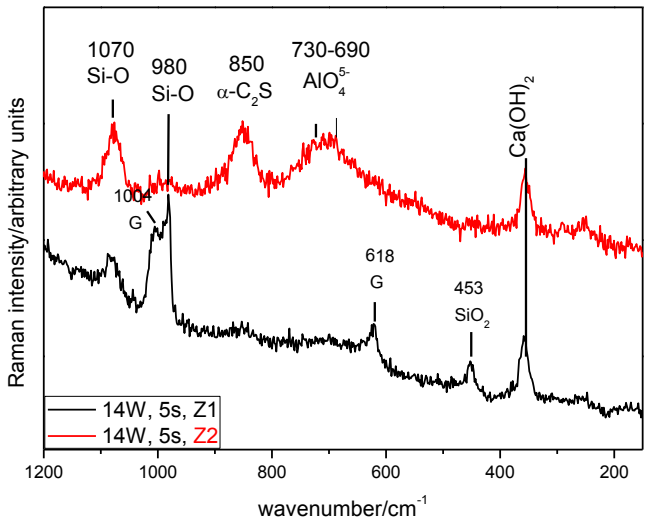

Fig. 3.- Micro-Raman spectra for zones Z1 and Z2 in the sample OPC-1 (14 W, 5 s) spot; G = gypsum

In Zone 2, which would have received dissipated heat, the main vibration bands appeared at 1070 cm^{-1} (broad), 850 cm^{-1} (broad), 730 cm^{-1} to 690 cm^{-1} (very broad) and 356 cm^{-1} (broad). As noted earlier, the broad band at 1070 cm^{-1} might have been generated by tetrahedral Si-O symmetrical stretching. The very broad band at 730 cm^{-1} to 690 cm^{-1} was generated by aluminates, for according to several authors [21, 23-26],

the main Raman aluminate bands in anhydrous cement phase C_4AF lie at 506 cm^{-1} (ν_1 [AlO_4^{5-}]) and 730-690 cm^{-1} (ν_3 [AlO_4^{5-}]). The sample can consequently be assumed to have been heated to 1200 °C to 1300 °C at which these aluminate phases form [27].
The broad band peaking at 850 cm^{-1} was associated with α-C_2S[3] [28].

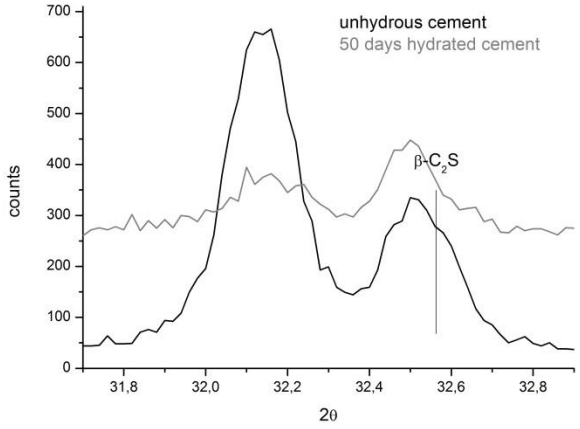

Fig. 4.- XRD patterns (2θ = 31.7-32.9°) for anhydrous and 50 d hydrated mortar samples

Whilst initially the cement contained both C_3S and β-C_2S, as the hydration rate is higher in C_3S, the 50 d sample contained primarily the latter (Figures 1 and 4). After laser radiation, β-C_2S converted to α-C_2S further to the Ca_2SiO_4 phase transformation flowchart shown in Scheme 1 [27], an indication that the temperature in Z2 peaked at around 1400 °C.

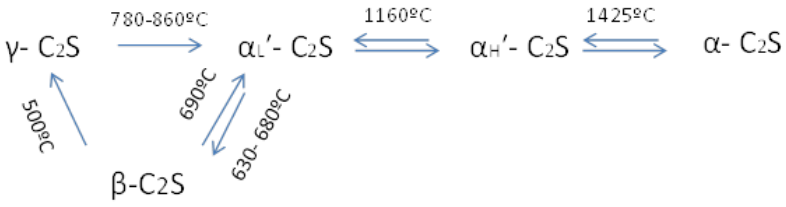

Scheme 1.- Ca_2SiO_4 transformation with temperature

[3] Cement chemistry notation: C = CaO; S = SiO_2; H = H_2O; A = Al_2O_3; F = Fe_2O_3

The presence in both Z1 and Z2 of a broad band peaking at 350 cm^{-1} and a narrow band at 3616 cm^{-1} (area not shown on the Raman spectrum) attested to portlandite formation in both zones. That finding was consistent with earlier reports of its presence in CO_2 laser-irradiated pozzolan mortars [8, 10]. Prior research [10] showed that portlandite formed in OPC after vacuum radiation, inferring that CaO reacted with radiation-induced water vapour.

The presence of distinctly different compounds in the core and adjacent ring regions of sample OPC-1 may be an indication of different peak temperatures: higher (1700 °C) in Z1, where the laser beam impacted, and lower in Z2 (~1400 °C), the heat dissipation zone.

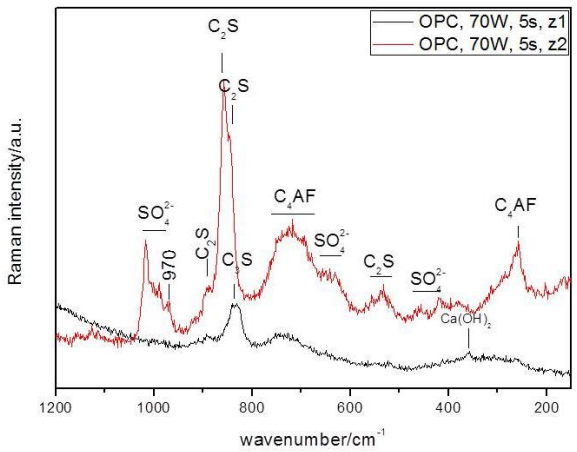

Fig. 5.- Micro-Raman spectra for zones Z1 and Z2 in the sample OPC-5 (70 W, 5 s) spot

In OPC-5, exposed to higher power (70 W, 5 s) laser radiation, the most prominent Raman signal on the spectrum for Z1, at 850 cm^{-1}, was generated by Si-O stretching vibrations in C_3S, whereas that signal shifted to higher wavenumbers in Z2. The double band at 857 cm^{-1} and 845 cm^{-1} in the Z2 spectrum was associated with the Si-O stretching vibrations in β-C_2S, attesting to the formation of that calcium silicate phase [14]. Those findings may denote a high cooling rate, for β-C_2S formation calls for rapid

cooling to elude transformation to γ-C_2S. Calcium sulfate-related bands in the form of anhydrite were also observed, along with the signals characteristic of the aluminoferrite (C_4AF) vibrations induced at 1200 °C to 1300 °C. As noted earlier, the extent of anhydrite hydration depends on temperature and formation rate. In light of anhydrite formation in Z2, the temperature reached may be assumed to have been higher than in the Z2 in previous point with less laser power (14 W, 5 s).

Furthermore a small resonance with maximum at 970 cm^{-1} can be an indication of another calcium silicate phase formed. When cement is exposed to temperatures of over 800 ºC, C-S-H decomposes [4] into belite (C2S) and wollastonite (CS). Belite was observed in Z2 in the sample exposed to 70 W CO_2 laser radiation, whilst the resonance at 970 cm^{-1} might have been generated by wollastonite [29]. Taken together, these findings would denote water loss after radiation and the formation of CS, C_2S and C_3S.

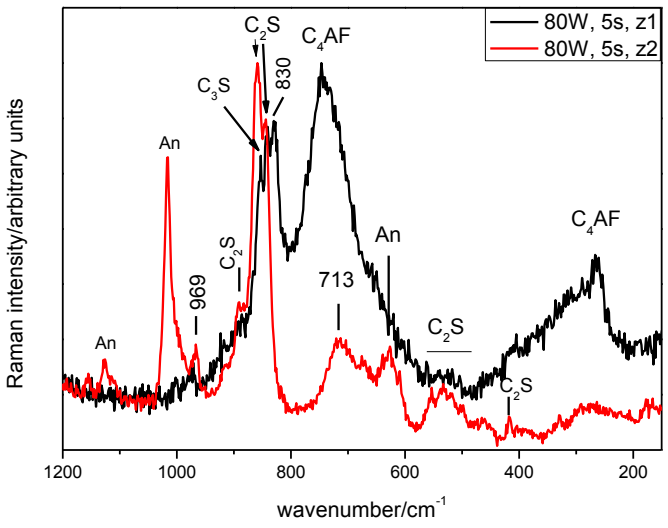

Fig. 6.- Micro-Raman spectra for zones Z1 and Z2 in the sample OPC-7 (80 W, 5 s) spot

Silicate phases such as β-C_2S as well as anhydrite were identified on the spectrum for Z2 in the samples exposed to 80 W laser radiation (Figure 6), whereas in the core region of the spot (Z1) the main phases were C_3S and C_4AF. An intense band at 830 cm^{-1} on the

Raman spectra may have denoted the formation of another calcium silicate phase. The absence of a signal attributable to quartz would imply that the temperatures reached exceeded its 1710 °C melting point.

The resonance at 969 cm^{-1} may have been generated by the very stable anhydrite [19] formed at T>1180 °C. No gypsum was detected on the 80 W, 5 s spectra.

The phases identified and the estimated surface temperature in the two zones of the irradiated samples are summarised in Table 2.

Table 2.- Phases identified in Z1 and Z2 of the irradiated samples

Sample	Raman-identified phase		Estimated surface temperature (°C)	
	z1	z2	z1	z2
OPC-1 (14 W)	gypsum, $Ca(OH)_2$, SiO_2	α-C_2S^*, C_4AF^*, $Ca(OH)_2$	1700 (no quartz)	1400 (fast cooling)
OPC-5 (70 W)	C_3S^*, $Ca(OH)_2$	β-C_2S^*; C_4AF^*; $CaSO_4$	1700 (no quartz)	1300 (fast cooling)
OPC-7 (80 W)	C_3S^*, C_4AF^*	β-C_2S^*; C_4AF^*; $CaSO_4$	1700 (no quartz)	1300 (fast cooling)

*Cement chemistry notation C: CaO; S = SiO_2; A = Al_2O_3; F = Fe_2O_3

A comparison of the 940 cm^{-1} to 780 cm^{-1} interval on the Raman spectra for Z1 and Z2 showed that the SiO_4 stretching band shifted with rising laser power, more visibly in Z1 (Figure 7), attesting to variations in the silicate structure. In pure β-C_2S the primary symmetrical stretching bands lie at 854±5 cm^{-1} and 841±5 cm^{-1}, whilst in pure C_3S they peak at 849±5 cm^{-1} and 839 ±5 cm^{-1} [14, 23, 24]; i.e., both bands lie at higher wavenumbers in the former than in the latter.

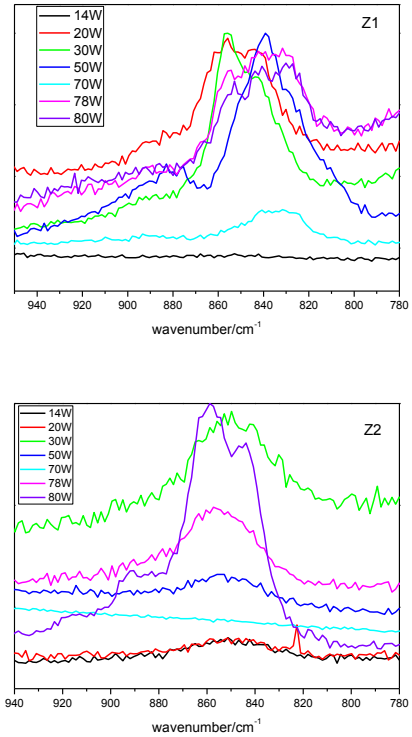

Fig. 7.- Micro-Raman spectra for Z1 (top) and Z2 (bottom) after 14 W to 80 W CO_2 laser radiation

Raman band shifts may be attributed to changes in compound microstructure, in the form of either impurity uptake, which is known to stabilise calcium silicate polymorphs, or variations in the Ca/Si ratio [28].The latter would infer the existence of two distinct compounds, such as C_3S and C_2S. Inasmuch as one or the other formed when the mortar was laser irradiated, the band shifts observed here should be attributed such differences in the Ca/Si ratio. The Si-O bond stretching bands (at 854 cm^{-1} and 839 cm^{-1}) depicted in Figure 8, resulting from the deconvolution of the Raman spectra in the interval 920 cm^{-1} to 820 cm^{-1}, shifted with rising laser power, downward in Z1 and upward in Z2. The conclusion drawn is that in the inner core of the irradiated sample C_3S formed at higher and C_2S at lower laser output. The opposite pattern was observed in the intermediate ring, where C_3S formed when laser radiation was applied at lower power.

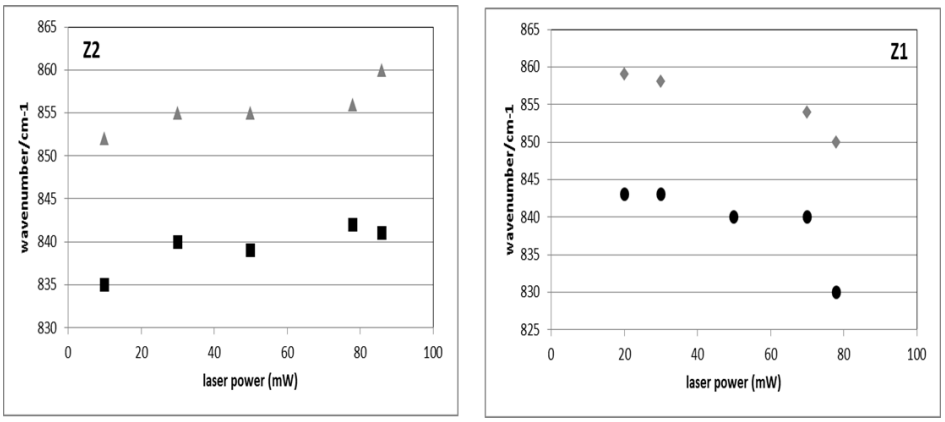

Fig. 8.- Variations in stretching band position vs laser power in exposure zones Z1 and Z2

CONCLUSIONS

This study showed that the composition of the anhydrous calcium silicate resulting from calcium silicate hydrate in laser irradiated cement depends on the laser power used. C_3S was identified in the inner core of irradiated spots, where the temperatures reached were higher, and C_2S in the Z2 zone, where the temperatures were lower. With rising laser power, the position of the Si-O bond stretching band shifted to higher values in the intermediate ring and lower values in the inner zone. The inference is that as power was raised, C_3S converted to C_2S in the core, and vice-versa in the ring. Tri- and dicalcium were consequently synthesised from calcium silicate hydrate along other than the usual pathway when CaO and SiO_2 are heated to 1200 °C- 1500 °C or hydrothermal procedures are deployed.

Calcium sulfate and C_4AF, other anhydrous phases, were also identified in the CO_2 laser-irradiated samples. The lowest power used, 14 W, induced the formation of anhydrite II. Stable at temperatures of under 1180 °C, this compound was subsequently hydrated with water vapour to yield gypsum. In contrast, anhydrite I, which is stable at temperatures over 1180 °C, formed at the highest power applied, 80 W. Hydration of the CaO present in the cement with the water vapour released in hydrated compound dehydration gave rise to $Ca(OH)_2$.

On the grounds of the phases formed and given the absence of quartz, the temperature in the inner zone was estimated to peak at around 1700 °C. The non-detection of γ-C_2S was indicative of rapid cooling from core to adjacent ring.

The authors declare that there is no conflict of interest.

ACKNOWLEDGEMENTS

This research was funded by the Regional Government of Madrid and the European Social Fund (Geomaterials Programme 2-S2013/MIT-2914).

REFERENCES

[1] Bashandy AA (2015) Performance of self-curing concrete at elevated temperatures. Indian J. Eng. Mater. Sci. 22:93-104.

[2] Carréa H, Hagerb I, Perlot C (2014) Contribution to the development of colorimetry as a method for the assessment of fire-damaged concrete. European Journal of Environmental and Civil Engineering 18 (10):1130-1144. http://dx.doi.org/10.1080/19648189.2014.883336

[3] Hachemi S and Ounis A (2015) Performance of concrete containing crushed brick aggregate exposed to different fire temperatures. European Journal of Environmental and Civil Engineering 19(7): 805-824.

http://dx.doi.org/10.1080/19648189.2014.973535.

[4] Nijland TG and Larbi JA (2001) Unraveling the temperature distribution in fire-damaged concrete by means of PFM microscopy: Outline of the approach and review of potentially useful reactions. Heron 46 [4]:253-264.

[5] Kodur N (2014) Properties of Concrete at Elevated Temperatures. ISRN Civil Engineering 14:1-15.

http://dx.doi.org/10.1155/2014/468510.

[6] Shaw S, Henderson CMB, Komanschek BU (2000) Dehydration/recrystallization mechanisms, energetics, and kinetics of hydrated calcium silicate minerals: an in situ TGA/DSC and synchrotron radiation SAXS/WAXS study. Chem. Geol. 167:141–159. http://dx.doi.org/10.1016/S0009-2541(99)00206-5.

[7] Tajuelo Rodríguez E, Garbev K, Merz D, Black L, Richardson IG (2017) Thermal stability of C-S-H phases and applicability of Richardson ad Grove´s and Richardson C-(A)-S-H (I) models to synthetic C-S-H. Cem Concr Res 93:45-56. http://dx.doi.org/10.1016/j.cemconres.2016.12.005

[8] Gómez-Heras M, Fort R, Morcillo M, Molpeceres C, Ocaña JL (2008) Laser heating: a minimally invasive technique for studying fire-generated heating in building stone. Mater. Construcc. 58(289-290): 203-217. DOI: 10.3989/mc.2008.v58.i289-290.82.

[9] Moreno-Virgen MR, Soto-Bernal JJ, Ortiz-Lozano JA, Bonilla-Petriciolet A, Vega-Durán JT, González-Mota R, Pineda-Piñón J (2011) Effect of CO_2 laser radiation on the mechanical properties of Portland cement pastes. Mater Construcc 61 (301):77-91. doi: 10.3989/mc.2010.54709.

[10] Martinez-Ramirez S, Diaz L, Camacho JJ (2013) CW CO_2-Laser-Induced Formation of Fulgurite on Lime–Pozzolan Mortar. J. Am. Ceram. Soc. 96[9]:2824–2830. DOI: 10.1111/jace.12515.

[11] Ishida H, Mabuchi K, Sasaki K, Mitsuda T (1992) Low-temperature synthesis of β-Ca_2SiO_4 from hillebrandite. J. Am. Ceram. Soc. 75:2427–2432. DOI: 10.1111/j.1151-2916.1992.tb05595.x.

[12] Bensted J (1976) Uses of Raman spectroscopy in cement chemistry. J. Am. Ceram. Soc. 59:140-143.

[13]. Bensted J (1977) Raman spectral studies of carbonation phenomena. Cem. Concr. Res. 7: 161-164.

[14] Ibañez J, Artús Ll, Cuscó R, López A, Menéndez E, Andrade MC (2007). Hydration and carbonation of monoclinic C2S and C3S studied by Raman spectroscopy. J. Raman Spectrosc 38:61-67. Doi:10.1002/jrs.1599.

[15] Renaudin G, Russias J, Leroux F, Cau-dit-Coumes C, Frizon F (2009). Journal of Solid State Chemistry 182:3320–3329. doi:10.1016/j.jssc.2009.09.024.

[16] Newman SP, Clifford SJ, Coveney PV, Gupta V, Blanchard JD, Serafin F, Ben-Amotz D, Diamond S (2005) Anomalous fluorescence in near-infrared Raman spectroscopy of cementitious materials. Cement and Concrete Research 35: 1620-1628. Doi:10.1016/j.cemconres.2004.10.001.

[17] Lawrence J (2004) A Comparative Analysis of the Wear Characteristics of Glazes Generated on the Ordinary Portland Cement Surface of Concrete by Means of CO_2 and High Power Diode Laser Radiation. Wear 257:590–598.

[18] Carter EA, Pasek MA, Smith T, Kee T, Pines P, Edwards HGM (2010). Rapid Raman mapping of a fulgurite. Anal Bioanal Chem 397:2647–2658. DOI 10.1007/s00216-010-3593-z

[19] Prieto-Taboada N, Gómez-Laserna O, Martínez-Arkarazo I, Olazabal MA, Madariaga JM (2014). Raman spectra of the different phases in the $CaSO_4$–H_2O system. Anal. Chem. 86:10131−10137. dx.doi.org/10.1021/ac501932f.

[20] Sanz Arauz D. Análisis del yeso empleado en revestimientos exteriores mediante técnicas geológicas. PhD Madrid (2009).

[21] Colomban P, Paulsen O (2005) Non-Destructive Determination of the Structure and Composition of Glazes by Raman Spectroscopy. J. Am. Ceram. Soc. 88(2):390-395. DOI: 10.1111/j.1551-2916.2005.00096.x.

[22] Bates JB (1972). Raman Spectra of α and β-Cristobalite. The Journal of Chemical Physics 57(9):4040-4047.

[23] Torréns-Martín D, Fernández-Carrasco L, Martínez-Ramírez S (2013a) Hydration of calcium aluminates and calcium sulfoaluminate studied by Raman spectroscopy. Cem. Concr. Res., 47:43–50. DOI: 10.1016/j.cemconres.2013.01.015.

[24] Torrens-Martin D, Fernandez-Carrasco L, Martinez-Ramirez S, Ibañez J, Artus Ll, Matschei T (2013b) Raman Spectroscopy of Anhydrous and Hydrated Calcium Aluminates and Sulfoaluminates. J. Am. Ceram. Soc., 96(11):3589–3595. DOI: 10.1111/jace.12535.

[25] Black L, Breen Ch, Yarwood J, Deng CS, Phippsb J, Maitland G (2006) Hydration of tricalcium aluminate (C_3A) in the presence and absence of gypsum—studied by Raman spectroscopy and X-ray diffraction. J. Mater. Chem., 16:1263–1272. DOI: 10.1039/B509904H.

[26] Kajihara K, Matsuishi S, Hayashi K, Hirano M, Hosono H (2007) Vibrational Dynamics and Oxygen Diffusion in a Nanoporous Oxide Ion Conductor $12CaO \cdot 7Al_2O_3$ Studied by ^{18}O Labeling and Micro-Raman Spectroscopy. J. Phys. Chem. C, 111:14855-14861. DOI: 10.1021/jp074248n.

[27] Taylor HFW (1990). Cement Chemistry. Academic Press, New York, 1990.

[28] Remy C, Reynard B, Madon M (1997)0 Raman Spectrosocpic Investigations of Dicalcium Silicate: Polymorphs and High-Temperature Phase Transformations. J. Am. Ceram. Soc 80(2):413-423. DOI: 10.1111/j.1151-2916.1997.tb02846.x.

[29] Handke M (1986) Vibrational Spectra, Force Constants, and Si-O Bond Character in Calcium Silicate Crystals Structure. Applied Spectroscopy 40 (6): 871-877.